


Effects of the viscoelastic interface bonding on a thickness-shear mode circular cylindrical piezoelectric transformer

Peng Li and Feng Jin

Journal of Intelligent Material Systems and Structures
24(15) 1888–1896
© The Author(s) 2013
Reprints and permissions:
sagepub.co.uk/journalsPermissions.nav
DOI: 10.1177/1045389X13486711
jim.sagepub.com


Abstract

A cylindrical piezoelectric transformer with an imperfect interface operating with thickness-shear modes is used within the three-dimensional equations of piezoelectricity. The shear–slip interface model is used to simulate the effect of viscoelastic imperfect interface. The influence of interface parameters on the transforming ratio, input admittance, power density, efficiency, and the displacement and stress distributions along the radius direction is discussed. Numerical results show that the weak interface lowers the performance of the transformer overall, which may provide theoretical guidance for the design of piezoelectric transformers.

Keywords

Piezoelectric transformer, viscoelastic imperfect interface, resonance frequency, transforming ratio, input admittance, power density, efficiency

Introduction

Owing to the strong coupling property between the electrical and mechanical constitutive behaviors, piezoelectric materials have been made into several kinds of electronic devices (Benes et al., 1998; Duong and Garcia, 1996; Karlash, 2004; Stanton et al., 2011; Vellekoop, 1998), such as interdigital transducers (Vellekoop, 1998), energy harvesters (Stanton et al., 2011), transformers (Karlash, 2004), rotary actuators (Duong and Garcia, 1996), bulk acoustic wave (BAW) and surface acoustic wave (SAW) sensors (Benes et al., 1998), and so on. Totally, these piezoelectric devices have been integrated with structural materials to form a class of smart structures. Taking a transformer for instance, it is used to raise or lower a voltage using a piezoelectric material. Examples are computer backlights, florescent ballast, portable electronic chargers, ignition of gas-discharge lamps, and compact ac/dc and dc/dc converters (Yang and Wang, 2008). Compared with some electromagnetic ones, piezoelectric transformers are more suitable in certain low-power applications. More references about transformers can be found in a review article (Yang, 2007).

Usually, the piezoelectric transformers contain at least two portions, that is, input and output parts. From another perspective, these piezoelectric two-layered or multilayered composite structures are common in

electronic devices. Very often a gluing substance, for example, epoxy, is applied to the interfaces (Wu and Liu, 1999). Besides, the interface in piezoelectric sensors may be damaged under harsh conditions, which would in turn affect the electromechanical behaviors of the sensors (Cao et al., 2009). Meanwhile, due to various causes such as microdefect, diffusion impurity, and damage, two dissimilar materials cannot be perfectly bonded. The weakened interfacial continuity affects device performance, in particular interfacial characteristics (Termonia, 1990). Therefore, in the designs and applications of piezoelectric sensors, it is necessary to take the possible imperfect interface into consideration.

Researchers have developed imperfect interface models with different levels of sophistication (Dybwad, 1985; Jin et al., 2005; Lavrentyev and Rokhlin, 1998; Leungvicharoen and Wijeyewickrema, 2003; Li and Lee, 2010; Melkumyan and Mai, 2008; Murtya, 1975; Nagy, 1992; Pang and Liu, 2011; Wang et al., 2000). The simplest description is to treat it as a layer that

State Key Laboratory for Strength and Vibration of Mechanical Structures, Xi'an Jiaotong University, Xi'an, China

Corresponding author:

Feng Jin, State Key Laboratory for Strength and Vibration of Mechanical Structures, Xi'an Jiaotong University, Xi'an, Shaanxi 710049, China.
Email: jinfengzhao@263.net

geometrically has a zero thickness but still possesses elasticity and interface elastic strain energy, for example, a shear-lag model (Li and Lee, 2010; Melkumyan and Mai, 2008; Pang and Liu, 2011), in which the tangential displacement at the interface is allowed to be different from both sides of the interface in order to account for the deformation of the interface layer. Mechanical and electrical properties and behaviors of weak interfaces described by different models have been widely studied theoretically (Dybwad, 1985; Li and Lee, 2010; Melkumyan and Mai, 2008; Pang and Liu, 2011) and experimentally (Jin et al., 2005; Lavrentyev and Rokhlin, 1998). More references about the imperfect interface can be found in a few review articles (Nagy, 1992; Wang et al., 2000).

To the authors' best knowledge, few work has been carried out so far to discuss the effect of imperfect interface on the behavior of a piezoelectric transformer. However, this is significant for the design of high-quality electronic devices. In the present contribution, the shear-slip interface model is used to simulate the effect of viscoelastic imperfect interface on a cylindrical piezoelectric ceramic transformer. First, the governing equations, boundary and continuous conditions, and exact solution of thickness-shear modes in the cylindrical piezoelectric transformer are given in Section "Theoretical analysis of the cylindrical piezoelectric transformer". Then, the influence of viscoelastic imperfect interface on the performance of the transformer is simulated based on the solution obtained. Finally, some conclusions are drawn.

Theoretical analysis of the cylindrical piezoelectric transformer

Consider a piezoelectric circular cylinder of polarized ceramics (see Figure 1) with the z -axis being the poling direction or the sixfold axis. The cylinder is unbounded in the z -direction. A polar coordinate system is defined by $x = r\cos\theta$ and $y = r\sin\theta$. The inner and outer faces at $r = a, b$ are traction free. There are three electrodes at $r = a, b, c$. The electrode at $r = c$ is grounded as a reference, and this interface is weakly bonded. Usually, time-harmonic driving voltage V_1 is applied across the electrodes at $r = a, c$. Due to the particular material orientation, the cylinder is driven into axial thickness-shear vibration, and an output voltage V_2 can be picked up across the electrodes at $r = c, b$, which are joined by a load circuit whose impedance is Z . In the next section, we mainly investigate the effect of the imperfectly bonded interface on the thickness-shear vibration in the transversely isotropic piezoelectric transformer. Since the material tensors of crystals of 6-mm symmetry have the same structures as polarized ceramics, our analysis is also valid for 6-mm piezoelectric crystals. This includes widely used materials such as ZnO and AlN (Qin et al., 2010; Zhang et al., 2009).

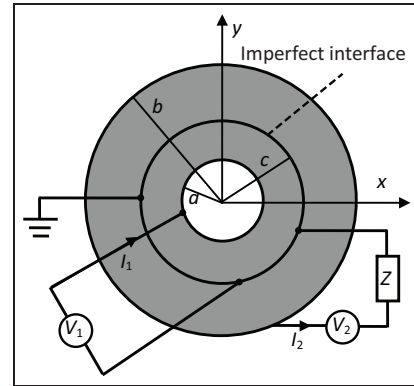


Figure 1. A cylindrical piezoelectric ceramic transformer with an imperfect interface.

The displacement components and electrical potential function of axial thickness-shear modes, which belongs to antiplane or shear horizontal (SH) motions, can be described as (Kielczynski et al., 2012)

$$u_x = u_y = 0, \quad u_z = u(x, y, t), \quad \varphi = \varphi(x, y, t) \quad (1)$$

Therefore, the governing equations can be obtained as

$$\begin{aligned} c_{44}\nabla^2 u + e_{15}\nabla^2 \varphi &= \rho \frac{\partial^2 u}{\partial t^2} \\ e_{15}\nabla^2 u - \varepsilon_{11}\nabla^2 \varphi &= 0 \end{aligned} \quad (2)$$

where c_{44} , e_{15} , ε_{11} , and ρ stand for the elastic constant, the piezoelectric, the dielectric permittivity coefficients, and mass density of the piezoelectric material, respectively. The boundary and interfacial conditions are

$$\begin{aligned} r = a : T_{rz} &= 0, \quad \varphi = V_1, \\ r = b : T_{rz} &= 0, \quad \varphi = V_2, \\ r = c : \begin{cases} \varphi(c^+) = \varphi(c^-) = 0, \\ T_{rz}(c^+) = T_{rz}(c^-) = K[u(c^+) - u(c^-)] \end{cases} \end{aligned} \quad (3)$$

Here, we adopt the shear-slip interface model to calculate the influence of viscoelastic imperfect interface. When $K = 0$, the two parts lose their mechanical interaction and the case of $K = \infty$ is for the perfect interface with continuous displacement across the joint (Dybwad, 1985; Jin et al., 2005; Lavrentyev and Rokhlin, 1998; Li and Lee, 2010; Melkumyan and Mai, 2008; Pang and Liu, 2011). Considering the axisymmetric motions independent of θ , which means $u_z = u(r, t)$ and $\varphi = \varphi(r, t)$ (Chen et al., 2009; Yang et al., 2007), $\nabla^2 = (\partial^2/\partial r^2) + 1/r(\partial/\partial r)$ can be obtained. For harmonic motions, we use the complex notation

$$\begin{aligned} [u, \varphi, T_{rz}, D_r, I_1, V_1, Q_1, I_2, V_2, Q_2] \\ = \text{Re}\{(U, \Phi, T, D, \bar{I}_1, \bar{V}_1, \bar{Q}_1, \bar{I}_2, \bar{V}_2, \bar{Q}_2) \exp(i\omega t)\} \end{aligned} \quad (4)$$

where $U, \Phi, T, D, \bar{I}_1, \bar{V}_1, \bar{Q}_1, \bar{I}_2, \bar{V}_2,$ and \bar{Q}_2 are complex variables. Therefore, the governing equations can be written as

$$\frac{\partial^2 U}{\partial r^2} + \frac{1}{r} \frac{\partial U}{\partial r} = -\xi^2 U \quad (5)$$

where the wavenumber $\xi = \omega / \sqrt{\bar{c}_{44} / \rho}$ with the effective piezoelectric stiffness $\bar{c}_{44} = c_{44} + (e_{15}^2 / \varepsilon_{11})$. The boundary and interfacial conditions in equation (3) can be expressed with the complex notation

$$\begin{aligned} r = a : T = 0, \Phi = \bar{V}_1, \\ r = b : T = 0, \Phi = \bar{V}_2, \\ r = c : \begin{cases} \Phi(c^+) = \Phi(c^-) = 0, \\ T(c^+) = T(c^-) = K[U(c^+) - U(c^-)] \end{cases} \end{aligned} \quad (6)$$

where the effective interface elastic stiffness parameter K (N/m³) is a complex variable, that is, $K = K_1 + iK_2$. K_1 and K_2 are simultaneously used to describe how well the two portions are bonded.

Based on the complex notation above, the displacement U , electrical potential function Φ , interface stress T , and electric displacement D are obtained as follows

$$U = \begin{cases} A_1 J_0(\xi r) + A_2 Y_0(\xi r), & a < r < c \\ B_1 J_0(\xi r) + B_2 Y_0(\xi r), & c < r < b \end{cases} \quad (7a)$$

$$\Phi = \begin{cases} \frac{e_{15}}{\varepsilon_{11}} [A_1 J_0(\xi r) + A_2 Y_0(\xi r)] + A_3 \ln r + A_4, & a < r < c \\ \frac{e_{15}}{\varepsilon_{11}} [B_1 J_0(\xi r) + B_2 Y_0(\xi r)] + B_3 \ln r + B_4, & c < r < b \end{cases} \quad (7b)$$

$$T = \begin{cases} -\bar{c}_{44} \xi [A_1 J_1(\xi r) + A_2 Y_1(\xi r)] + e_{15} \frac{A_3}{r}, & a < r < c \\ -\bar{c}_{44} \xi [B_1 J_1(\xi r) + B_2 Y_1(\xi r)] + e_{15} \frac{B_3}{r}, & c < r < b \end{cases} \quad (7c)$$

$$D = \begin{cases} -\varepsilon_{11} \frac{A_3}{r}, & a < r < c \\ -\varepsilon_{11} \frac{B_3}{r}, & c < r < b \end{cases} \quad (7d)$$

where $A_1, A_2, A_3, A_4, B_1, B_2, B_3,$ and B_4 are undermined coefficients. Substituting Equation (7) into Equation (6) gives

$$\begin{aligned} -\bar{c}_{44} \xi [A_1 J_1(\xi a) + A_2 Y_1(\xi a)] + e_{15} \frac{A_3}{a} &= 0, \\ -\bar{c}_{44} \xi [B_1 J_1(\xi b) + B_2 Y_1(\xi b)] + e_{15} \frac{B_3}{b} &= 0, \\ \frac{e_{15}}{\varepsilon_{11}} [A_1 J_0(\xi a) + A_2 Y_0(\xi a)] + A_3 \ln a + A_4 &= \bar{V}_1, \\ \frac{e_{15}}{\varepsilon_{11}} [B_1 J_0(\xi b) + B_2 Y_0(\xi b)] + B_3 \ln b + B_4 &= \bar{V}_2, \\ \frac{e_{15}}{\varepsilon_{11}} [A_1 J_0(\xi c) + A_2 Y_0(\xi c)] + A_3 \ln c + A_4 &= 0, \\ \frac{e_{15}}{\varepsilon_{11}} [B_1 J_0(\xi c) + B_2 Y_0(\xi c)] + B_3 \ln c + B_4 &= 0, \\ -\bar{c}_{44} \xi [A_1 J_1(\xi c) + A_2 Y_1(\xi c)] \\ + e_{15} \frac{A_3}{c} &= -\bar{c}_{44} \xi [B_1 J_1(\xi c) + B_2 Y_1(\xi c)] + e_{15} \frac{B_3}{c}, \\ -\bar{c}_{44} \xi [A_1 J_1(\xi c) + A_2 Y_1(\xi c)] \\ + e_{15} \frac{A_3}{c} &= K[(B_1 - A_1)J_0(\xi c) + (B_2 - A_2)Y_0(\xi c)] \end{aligned} \quad (8)$$

For the output electrode at $r = b$, the following charge can be obtained (Xu et al., 2009)

$$\bar{Q}_2 = - \int_0^{2\pi} D|_{r=b} b d\theta \quad (9)$$

Owing to the fact $I_2 = -\dot{\bar{Q}}_2$, the complex current is

$$\bar{I}_2 = i\omega \int_0^{2\pi} D|_{r=b} b d\theta = -2\pi i\omega \varepsilon_{11} B_3 \quad (10)$$

Hence, the relationship between the output voltage and current can be written as

$$\bar{V}_2 = \bar{I}_2 Z = -2\pi i\omega \varepsilon_{11} Z B_3 \quad (11)$$

Equations (8) and (11) contain nine equations with nine coefficients $A_1, A_2, A_3, A_4, B_1, B_2, B_3, B_4,$ and \bar{V}_2 . If the interface is perfect, that is, $K = \infty$, Equations (8) and (11) possess exactly the same expressions obtained in the work by Yang et al. (2007), which validates to some extent the accuracy of the theoretical derivation. Furthermore, these equations mentioned above can be simplified as

$$\begin{aligned} \left\{ k_e^2 [J_0(\xi a) - J_0(\xi c)] + a\xi \ln\left(\frac{a}{c}\right) J_1(\xi a) \right\} A_1 \\ + \left\{ k_e^2 [Y_0(\xi a) - Y_0(\xi c)] + a\xi \ln\left(\frac{a}{c}\right) Y_1(\xi a) \right\} A_2 = \frac{e_{15}}{\bar{c}_{44}} \bar{V}_1 \end{aligned} \quad (12a)$$

$$\begin{aligned} \left\{ k_e^2 [J_0(\xi b) - J_0(\xi c)] + b\xi \ln\left(\frac{b}{c}\right) J_1(\xi b) \left(1 + \frac{Z}{Z_0}\right) \right\} B_1 \\ + \left\{ k_e^2 [Y_0(\xi b) - Y_0(\xi c)] + b\xi \ln\left(\frac{b}{c}\right) Y_1(\xi b) \left(1 + \frac{Z}{Z_0}\right) \right\} B_2 = 0 \end{aligned} \quad (12b)$$

$$\begin{aligned} \left[\frac{a}{c} J_1(\xi a) - J_1(\xi c) \right] A_1 + \left[\frac{a}{c} Y_1(\xi a) - Y_1(\xi c) \right] A_2 \\ + \left[-\frac{b}{c} J_1(\xi b) + J_1(\xi c) \right] B_1 + \left[-\frac{b}{c} Y_1(\xi b) + Y_1(\xi c) \right] B_2 = 0 \end{aligned} \quad (12c)$$

$$\begin{aligned} \left\{ J_0(\xi c) + \Gamma \left[\frac{a}{c} J_1(\xi a) - J_1(\xi c) \right] \right\} A_1 \\ + \left\{ Y_0(\xi c) + \Gamma \left[\frac{a}{c} Y_1(\xi a) - Y_1(\xi c) \right] \right\} A_2 \\ - J_0(\xi c) B_1 - Y_0(\xi c) B_2 = 0 \end{aligned} \quad (12d)$$

$$\begin{aligned} A_3 &= \frac{\bar{c}_{44}}{e_{15}} a\xi [A_1 J_1(\xi a) + A_2 Y_1(\xi a)], \\ B_3 &= \frac{\bar{c}_{44}}{e_{15}} b\xi [B_1 J_1(\xi b) + B_2 Y_1(\xi b)] \end{aligned} \quad (13)$$

where

$$k_e^2 = \frac{e_{15}^2}{\varepsilon_{11} \bar{c}_{44}}, Z_0 = \frac{1}{i\omega C_0}, C_0 = \frac{2\pi \varepsilon_{11}}{\ln(b/c)}, \Gamma = \frac{\bar{c}_{44} \xi}{K} \quad (14)$$

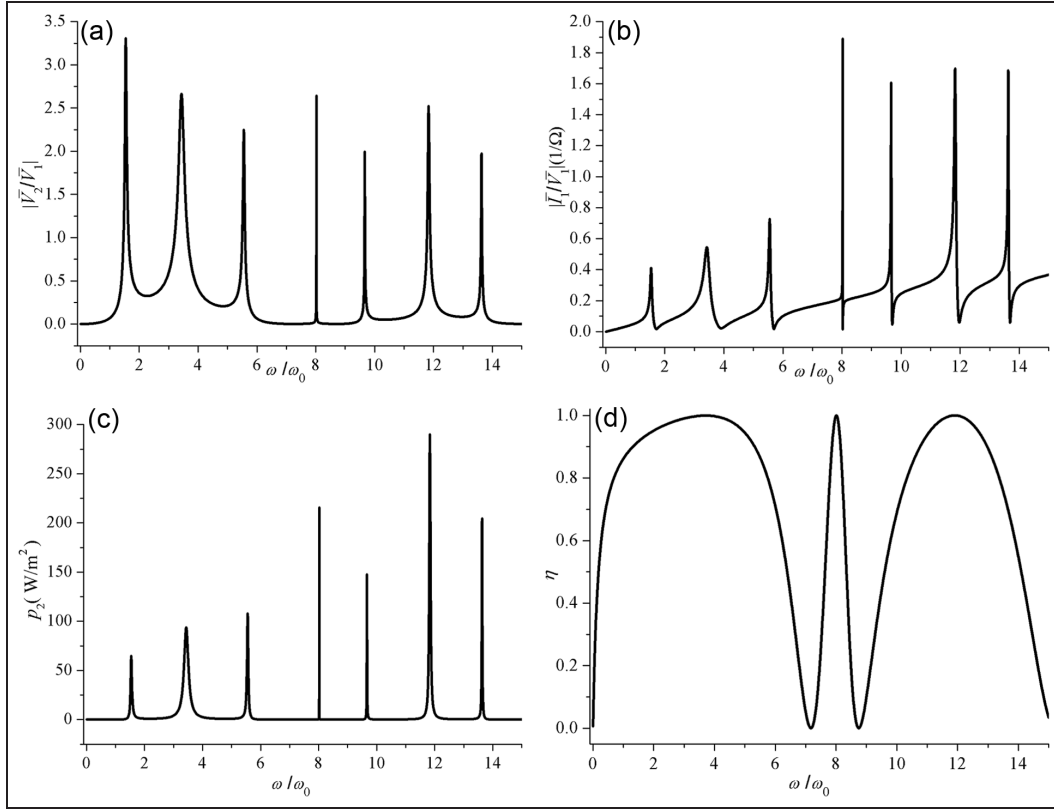


Figure 2. The first few resonances of (a) the transforming ratio $|\bar{V}_2/\bar{V}_1|$, (b) the admittance $|\bar{I}_1/\bar{V}_1|$, (c) the power density p_2 , and (d) the efficiency η versus the driving frequency ($\Gamma_1 = 0.5$, $\Gamma_2 = 1\% \Gamma_1$).

Equation (12) contains four equations with four undetermined coefficients A_1 , A_2 , B_1 , and B_2 . Once they are solved, the output voltage ratio $|\bar{V}_2/\bar{V}_1|$ can be obtained by using Equations (11) and (13). Similarly with output voltage and current, $I_1 = \dot{Q}_1$ can be easily obtained at $r = a$, and the input current satisfied

$$\bar{I}_1 = i\omega \int_0^{2\pi} D|_{r=a} ad\theta = -2\pi i\omega \varepsilon_{11} A_3$$

With the complex notation for harmonic motions, the input electrical power is given by (Xu et al., 2009)

$$P_1 = \frac{1}{4}(\bar{I}_1 \bar{V}_1^* + \bar{I}_1^* \bar{V}_1) \quad (15)$$

where an asterisk represents complex conjugate. The output electrical power is

$$P_2 = \frac{1}{4}(\bar{I}_2 \bar{V}_2^* + \bar{I}_2^* \bar{V}_2) \quad (16)$$

The efficiency of the transformer is defined as

$$\eta = \frac{P_2}{P_1} \quad (17)$$

Another quantity of practical interest is the power per unit volume (power density), which in our case may be calculated from

$$p_2 = \frac{P_2}{\pi b^2} \quad (18)$$

The effect of imperfect interface on the transformer

As a numerical example, consider a ceramic cylinder of PZT-5H with $c_{44} = 2.3 \times 10^{10}$ N/m², $e_{15} = 17$ C/m², $\varepsilon_{11} = 1.506 \times 10^{-8}$ F/m, and $\rho = 7500$ kg/m³ (Son and Kang, 2011). The additional load is fixed as $Z = (1 + i)Z_0$. The fundamental thickness-shear frequency of shell $\omega_0 = [\pi/2(b-a)]\sqrt{\bar{c}_{44}/\rho}$ is introduced during the following simulation for convenience. Since the interface glue is usually viscoelastic, we use a complex interface stiffness whose imaginary part describes interface damping. Consider $K = K_1 + iK_2$, where both K_1 and K_2 are real. Hence

$$\Gamma = \Gamma_1 - i\Gamma_2 = \frac{\bar{c}_{44}\xi}{K_1 + iK_2} = \frac{\bar{c}_{44}\xi}{|K|^2}(K_1 - iK_2) \quad (19)$$

where both Γ_1 and Γ_2 are real. Γ_1 is corresponding to the flexibility of the interface, while Γ_2 is the viscoelastic parameter. Hence, $\Gamma_1 = \Gamma_2 = 0$ is corresponding to the perfect interface.

Figure 2(a) to (d), respectively, shows the transforming ratio $|\bar{V}_2/\bar{V}_1|$, input admittance $|\bar{I}_1/\bar{V}_1|$, power density p_2 of the generated wave, and efficiency η versus

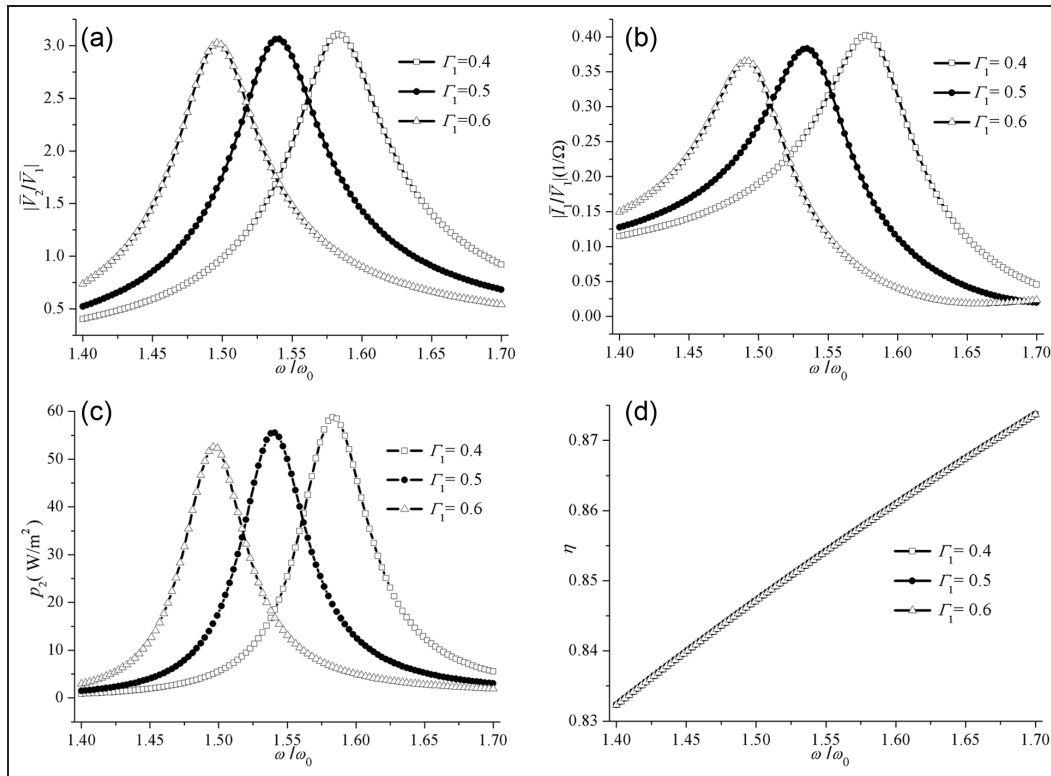


Figure 3. The first resonance of (a) the transforming ratio $|\bar{V}_2/\bar{V}_1|$, (b) the admittance $|\bar{I}_1/\bar{V}_1|$, (c) the power density p_2 , and (d) the efficiency η versus the driving frequency for some selected Γ_1 ($\Gamma_2 = 0.01$).

the driving frequency when the interface parameters satisfy $\Gamma_1 = 0.5$ and $\Gamma_2 = 1\% \Gamma_1$. The transforming ratio assumes its maxima at resonant frequencies as expected, which means the transformer is a resonant device operating at a particular frequency (Chen et al., 2009; Xu et al., 2009; Yang et al., 2007). Meanwhile, at resonances the admittance and output energy flux also assume maxima. Besides, the first resonance has the highest transforming ratio because, at higher resonance, the corresponding modes have nodal points, and some voltage cancellation usually occurs along the radius direction in the output portion of the transformer (Yang et al., 2007). The peak values of higher modes can be larger than the fundamental mode for the admittance and output energy flux, which can be seen from Figure 2(b) and (c). Therefore, it is found that the change of efficiency for the driving frequency is irregular.

Because the transform ratio achieves its maximum at the first resonance, we will focus on the effect of imperfect interface on the first mode of thickness-shear waves in the following discussion. The effects of the interface parameters Γ_1 and Γ_2 on the transforming ratio $|\bar{V}_2/\bar{V}_1|$, input admittance $|\bar{I}_1/\bar{V}_1|$, power density p_2 , and efficiency η near the first resonance locally are shown in Figures 3 and 4, respectively. The resonant frequency is sensitive to the interface parameter Γ_1 but insensitive to Γ_2 . The weak interface lowers the

frequency, which can be seen from Figure 3. Meanwhile, the amplitude of $|\bar{V}_2/\bar{V}_1|$, $|\bar{I}_1/\bar{V}_1|$, and p_2 of the first mode is smaller compared with the perfect interface. However, the efficiency η is sensitive to the interface parameter Γ_2 but insensitive to Γ_1 . Especially, when Γ_1 keeps constant, the efficiency does not change with the increasing driving frequency.

We suppose that the driving frequency follows the first resonant frequency when the interface changes in order to access the maximum amplitude of transforming ratio. Figures 5 and 6 show the varying patterns of $|\bar{V}_2/\bar{V}_1|$, $|\bar{I}_1/\bar{V}_1|$, p_2 , and η at the first resonance frequencies with the increasing of Γ_1 and Γ_2 for some special cases, respectively. These values all decrease when the interface becomes weak, which means the imperfect bonding interface has greater effect on the piezoelectric transformer. This kind of effect is harmful for us, and we must avoid the appearance of imperfect interface to our best.

The transforming ratio, input admittance, and efficiency all approach to zero with the increasing of Γ_1 . However, the limit value of input admittance is not zero. When $\Gamma_1 \rightarrow \infty$, the input and output piezoelectric parts have no mechanical connection and become two individual different portions. Therefore, no output voltage can be obtained in the outer piezoelectric circular cylinder, which is the reason that $|\bar{V}_2/\bar{V}_1|$, p_2 , and η approach to zero. However, the input voltage does not

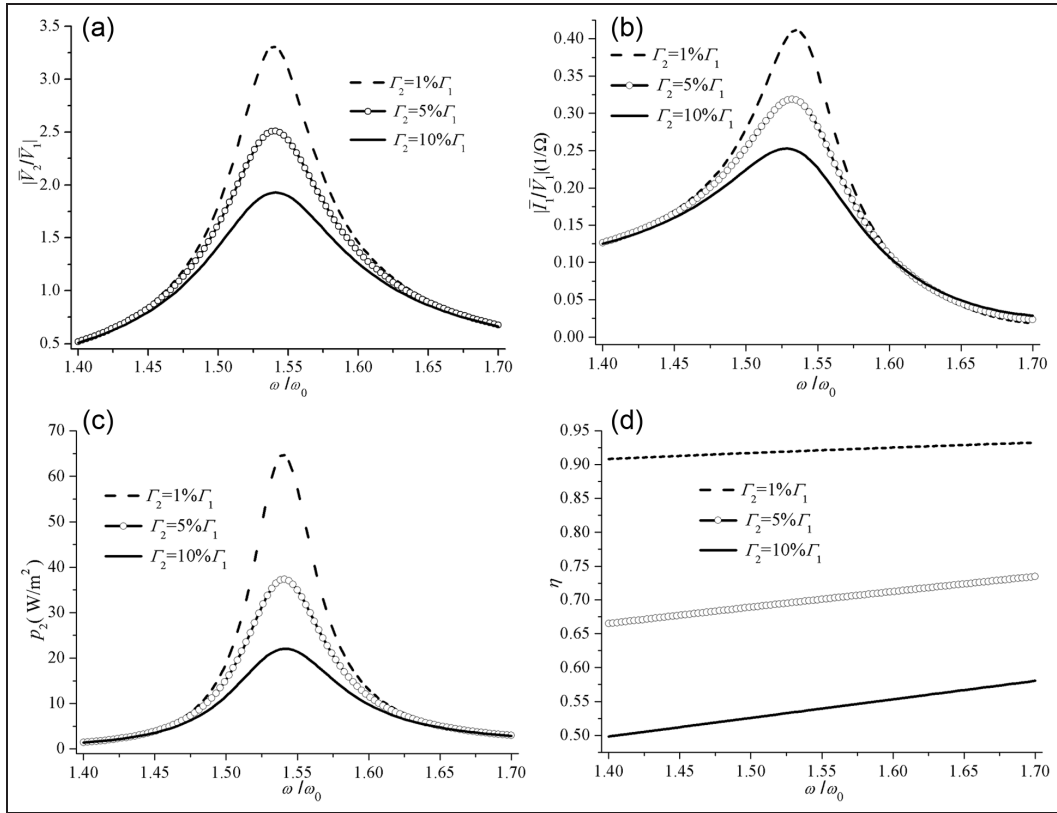


Figure 4. The first resonance of (a) the transforming ratio $|\bar{V}_2/\bar{V}_1|$, (b) the admittance $|\bar{I}_1/\bar{V}_1|$, (c) the power density p_2 , and (d) the efficiency η versus the driving frequency for some selected Γ_2 ($\Gamma_1 = 0.5$).

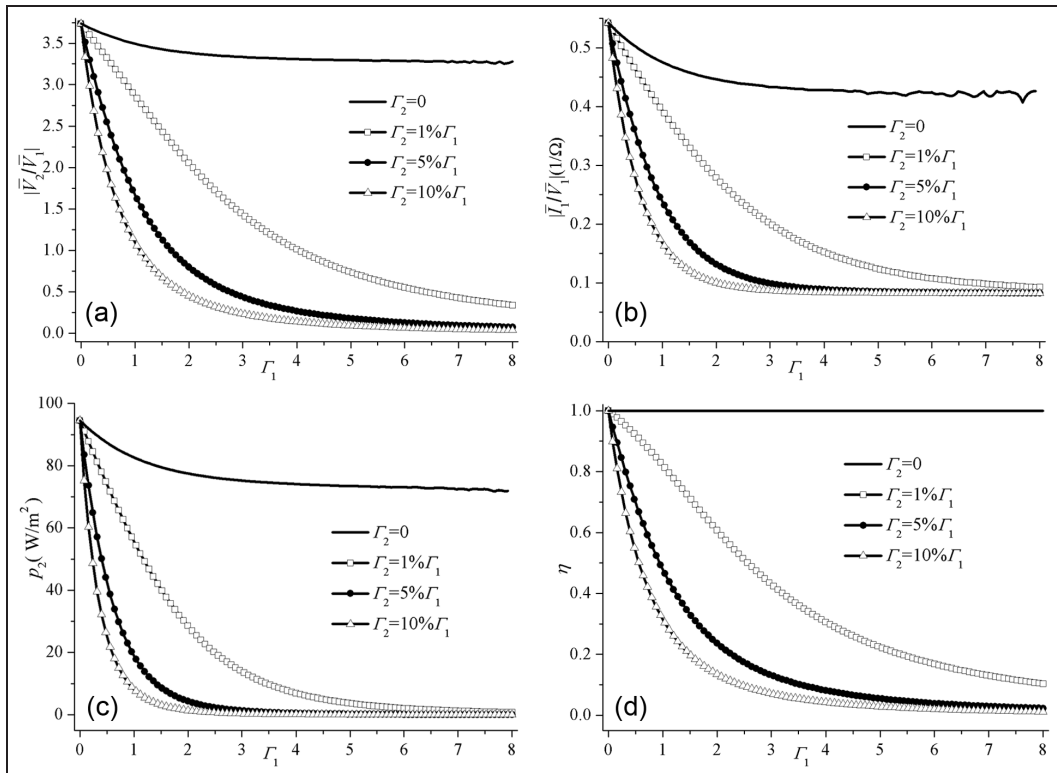


Figure 5. The first resonance of (a) the transforming ratio $|\bar{V}_2/\bar{V}_1|$, (b) the admittance $|\bar{I}_1/\bar{V}_1|$, (c) the power density p_2 , and (d) the efficiency η versus Γ_1 for some cases of Γ_2 .

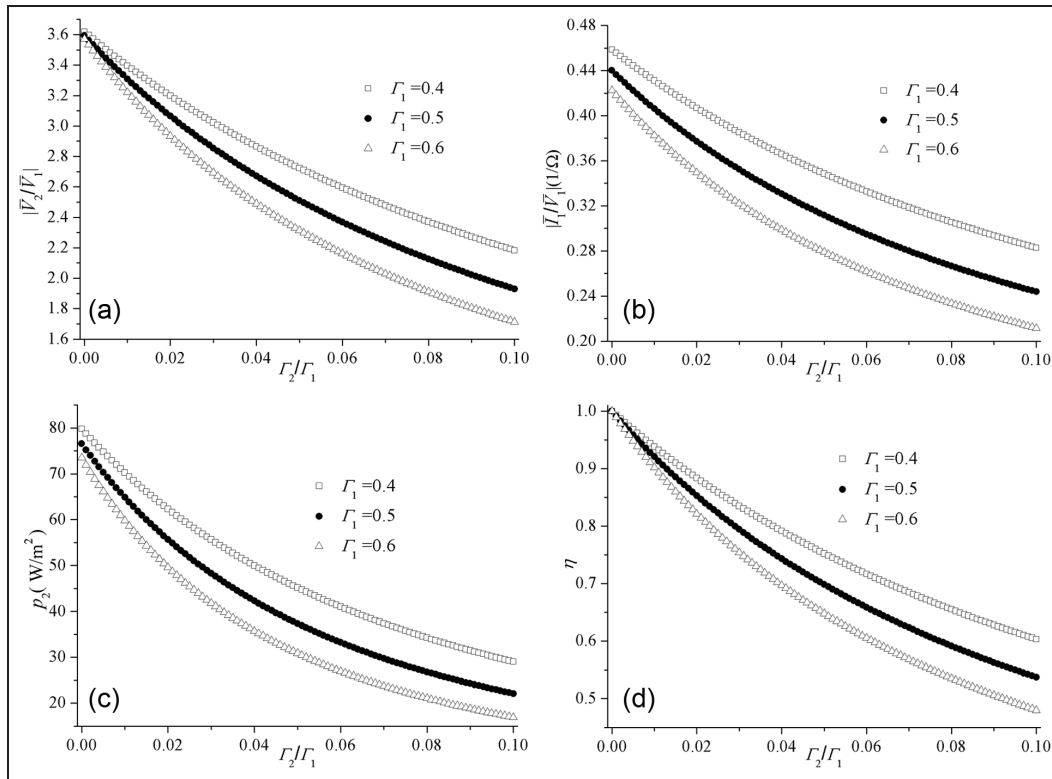


Figure 6. The first resonance of (a) the transforming ratio $|\bar{V}_2/\bar{V}_1|$, (b) the admittance $|\bar{I}_1/\bar{V}_1|$, (c) the power density p_2 , and (d) the efficiency η versus Γ_2/Γ_1 for some selected Γ_1 .

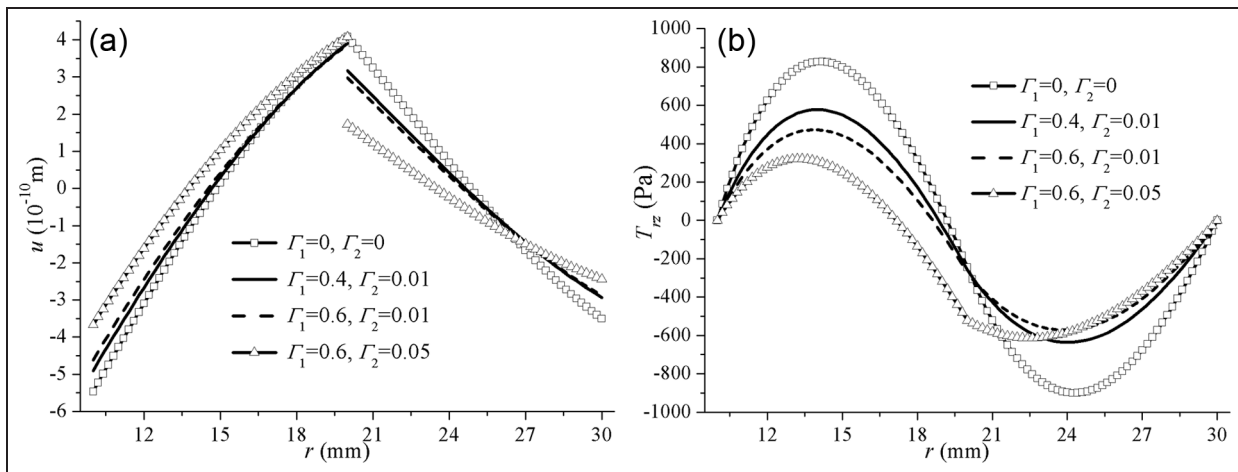


Figure 7. (a) The displacement distribution and (b) the stress distribution along the radius direction.

equal to zero, which leads to the finite limit value of $|\bar{I}_1/\bar{V}_1|$ at the circumstance of $\Gamma_1 \rightarrow \infty$. Besides, when $\Gamma_1 > 5$, each of the transforming ratio $|\bar{V}_2/\bar{V}_1|$, input admittance $|\bar{I}_1/\bar{V}_1|$, and power density p_2 has a fluctuation, which can be seen from Figure 5. Especially, the efficiency equals to unit when $\Gamma_2 = 0$, which is in accordance with Figure 3(d) and means no energy wastage during the transformation. Meanwhile, this outcome validates, to some extent, the correctness of the simulation results.

Similarly with the effect of Γ_1 , Γ_2 also lowers the maximum of the transforming ratio, input admittance, power density, and efficiency, which can be seen from Figure 6. Here, considering the fact that viscoelastic parameter Γ_2 is based on the value of Γ_1 , Γ_2 shifts in the range of 0%–10%.

Supposing that $V_1 = 1$ V, the distributions of the resonance displacement u and stress T_{rz} for the first mode along the radius direction are shown in Figure 7. Γ_1 and Γ_2 have the great effect on the displacement and

stress distributions. At the interface between the input and output parts, the displacement is discontinuous, as described by the shear–slip model. The stress keeps zero at the inner and outer edges whether the interface $r = c$ is perfect or not. Both Γ_1 and Γ_2 lower the maximum of stress distribution in the transformer. However, Γ_1 has no effect on the interface stress at $r = c$. In contrast, Γ_2 evidently increases the stress value at $r = c$, which needs to be considered during the application.

Overall, we have adopted the shear–slip model to describe the effect of imperfect interface on the performance of piezoelectric transformer. Besides, there are two kinds of linear viscoelasticity theories, that is, the Kelvin and Maxwell theories.

The displacement and stress conditions expressed at the imperfect interface $r = c$ in the present contribution are

$$T_{rz}(c^+) = T_{rz}(c^-) = k[u(c^+) - u(c^-)] + \gamma \frac{\partial}{\partial t} [u(c^+) - u(c^-)] \quad (20)$$

by the Kelvin theory (Fan and Wang, 2003) and

$$\left(\frac{1}{k} \frac{\partial}{\partial t} + \frac{1}{\gamma}\right) T_{rz}(c^+) = \left(\frac{1}{k} \frac{\partial}{\partial t} + \frac{1}{\gamma}\right) T_{rz}(c^-) = \frac{\partial}{\partial t} [u(c^+) - u(c^-)] \quad (21)$$

by the Maxwell theory (Fan and Wang, 2003). Based on the complex notation adopted in the present contribution, equations (20) and (21) can be obtained as follows

$$T(c^+) = T(c^-) = (k + i\gamma\omega)[U(c^+) - U(c^-)] \quad (22)$$

$$T(c^+) = T(c^-) = \left(\frac{k\gamma^2\omega^2}{k^2 + \gamma^2\omega^2} + i\frac{k^2\gamma\omega}{k^2 + \gamma^2\omega^2}\right) [U(c^+) - U(c^-)] \quad (23)$$

Hence, these two expressions above can be concluded by using the shear–slip model, that is

$$T(c^+) = T(c^-) = (K + iK_2)[U(c^+) - U(c^-)] \quad (24)$$

Here, the rate γ is coupled to the interface parameters, which cannot be seen directly from equation (24). Hence, the shear–slip model keeps in touch with the Kelvin and Maxwell theories in essence to a certain extent. Further research concerning the effect of viscoelastic interface bonding on the piezoelectric transformer by the Kelvin and Maxwell theories needs to be carried out in the future.

Conclusion

The shear–slip interface model is used to simulate the effect of viscoelastic imperfect interface on a thickness-

shear mode circular cylinder piezoelectric transformer. Overall, the weak interface evidently affects the transformer performance including the resonant frequency, transforming ratio, admittance, power density, efficiency, and displacement and stress distributions. Both Γ_1 and Γ_2 lower the transforming ratio, admittance, and power density compared with the perfect interface. Especially, the efficiency equals to unit when $\Gamma_2 = 0$. Meanwhile, they have great effect on the displacement and stress distributions. The displacement is noncontinuous at the interface, while the viscoelastic parameter Γ_2 increases the amplitude of interface stress. In short, the imperfect interface lowers the performance of the transformer, which needs to be considered in the further application. The theoretical and numerical results may provide guidance for the design of circular cylinder piezoelectric transformer when an imperfect interface appears.

Declaration of conflicting interests

The authors declare that there is no conflict of interest.

Funding

This work was supported by the National Natural Science Foundation of China (No. 11272247), the National 111 Project of China (No. B06024), and Scholarship Award for Excellent Doctoral Student granted by Ministry of Education.

References

- Benes E, Groschl M, Seifert F, et al. (1998) Comparison between BAW and SAW sensor principles. *IEEE Transactions on Ultrasonics Ferroelectrics and Frequency Control* 45: 1314–1330.
- Cao XS, Jin F and Jeon I (2009) Rayleigh surface wave in a piezoelectric wafer with subsurface damage. *Applied Physics Letters* 95: 261906.
- Chen WQ, Lv CF, Yang JS, et al. (2009) A circular cylindrical, radially polarized ceramic shell piezoelectric transformer. *IEEE Transactions on Ultrasonics Ferroelectrics and Frequency Control* 56: 1238–1245.
- Duong K and Garcia E (1996) Design and performance of a rotary motor driven by piezoelectric stack actuators. *Japanese Journal of Applied Physics* 35: 6334–6341.
- Dybwad GL (1985) A sensitive new method for the determination of adhesive bonding between a particle and a substrate. *Journal of Applied Physics* 58: 2789–2790.
- Fan H and Wang GF (2003) Interaction between a screw dislocation and viscoelastic interfaces. *International Journal of Solids and Structures* 40: 763–776.
- Jin F, Kishimoto K, Inoue H, et al. (2005) Experimental investigation on the interface properties evaluation in piezoelectric layered structures by Love waves propagation. *Key Engineering Materials* 297: 807–812.
- Karlash VL (2004) Electroelastic vibrations and transformation ratio of a planar piezoceramic transformer. *Journal of Sound and Vibration* 277: 353–367.

- Kielczynski P, Szalewski M and Balcerzak A (2012) Effect of a viscous liquid loading on Love wave propagation. *International Journal of Solids and Structures* 49: 2314–2319.
- Lavrentyev AI and Rokhlin SI (1998) Ultrasonic spectroscopy of imperfect contact interfaces between a layer and two solids. *Journal of the Acoustical Society of America* 103: 657–664.
- Leungvichcharoen S and Wijeyewickrema AC (2003) Dispersion effects of extensional waves in pre-stressed imperfectly bonded incompressible elastic layered composite. *Wave Motion* 38: 311–325.
- Li YD and Lee KY (2010) Effect of an imperfect interface on the SH wave propagating in a cylindrical piezoelectric sensor. *Ultrasonics* 50: 473–478.
- Melkumyan A and Mai YW (2008) Influence of imperfect bonding on interface waves guided by piezoelectric/piezomagnetic composites. *Philosophical Magazine* 88: 2965–2977.
- Murtya GS (1975) A theoretical model for the attenuation and dispersion of Stoneley waves at the loosely bonded interface of elastic half space. *Physics of the Earth and Planetary Interiors* 11: 65–79.
- Nagy PB (1992) Ultrasonic classification of imperfect interfaces. *Journal of Nondestructive Evaluation* 11: 127–139.
- Pang Y and Liu JX (2011) Reflection and transmission of plane waves at an imperfectly bonded interface between piezoelectric and piezomagnetic media. *European Journal of Mechanics A: Solids* 30: 731–740.
- Qin LF, Chen QM, Cheng HB, et al. (2010) Analytical study of dual-mode thin film bulk acoustic resonators (FBARs) based on ZnO and AlN films with tilted c-axis orientation. *IEEE Transactions on Ultrasonics Ferroelectrics and Frequency Control* 57: 1840–1853.
- Son MS and Kang YJ (2011) Propagation behavior of SH waves in layered piezoelectric plates. *Journal of Mechanical Science and Technology* 25: 613–619.
- Stanton SC, Erturk A, Mann BP, et al. (2011) Nonlinear non-conservative behavior and modeling of piezoelectric energy harvesters including proof mass effects. *Journal of Intelligent Material Systems and Structures* 23: 183–199.
- Termonia Y (1990) Fibre coating as a means to compensate for poor adhesion in fibre-reinforced materials. *Journal of Materials Science* 25: 103–106.
- Vellekoop MJ (1998) Acoustic wave sensors and their technology. *Ultrasonics* 36: 7–14.
- Wang YS, Yu GL, Zhang ZM, et al. (2000) Review on elastic waves propagation under complex interface (interface layer) conditions. *Advances in Mechanics* 30: 378–389 (in Chinese).
- Wu TT and Liu YH (1999) Inverse determinations of thickness and elastic properties of a bonding layer using laser-generated surface waves. *Ultrasonics* 37: 23–30.
- Xu LM, Geng YL, Zhang Y, et al. (2009) Power transmission through an unbounded elastic plate using a finite piezoelectric actuator and a finite piezoelectric power harvester. *International Journal of Applied Electromagnetics and Mechanics* 29: 145–156.
- Yang JS (2007) Piezoelectric transformer structural modeling—a review. *IEEE Transactions on Ultrasonics Ferroelectrics and Frequency Control* 54: 1154–1170.
- Yang JS and Wang J (2008) Dynamic anti-plane problems of piezoceramics and applications in ultrasonics—a review. *Acta Mechanica Solida Sinica* 21: 207–220.
- Yang JS, Chen ZG and Hu YT (2007) Theoretical modeling of a thickness-shear mode circular cylinder piezoelectric transformer. *IEEE Transactions on Ultrasonics Ferroelectrics and Frequency Control* 54: 621–626.
- Zhang HF, Turner JA and Kosinski JA (2009) Analysis of thickness vibrations of c-axis inclined aluminum-nitrogen thin film resonators. *Integrated Ferroelectrics* 113: 95–108.